

DANA: Dimension-Adaptive Neural Architecture for Multivariate Sensor Data

Mohammad Malekzadeh*, Richard G. Clegg, Andrea Cavallaro, Hamed Haddadi

Abstract—Motion sensors embedded in wearable and mobile devices allow for dynamic selection of sensor streams and sampling rates, enabling useful applications, *e.g.* for power management or control of data sharing. While deep neural networks (DNNs) achieve competitive accuracy in sensor data classification, current DNN architectures only process data coming from a fixed set of sensors with a fixed sampling rate, and changes in the dimensions of their inputs cause considerable accuracy loss, unnecessary computations, or failure in operation. To address this problem, we introduce a *dimension-adaptive pooling* (DAP) layer that makes DNNs robust to temporal changes in sampling rate and in sensor availability. DAP operates on convolutional filter maps of variable dimensions and produces an input of fixed dimensions suitable for feedforward and recurrent layers. Building on this architectural improvement, we propose a *dimension-adaptive training* (DAT) procedure to generalize over the entire space of feasible data dimensions at the inference time. DAT comprises the random selection of dimensions during the forward passes and optimization with accumulated gradients of several backward passes. We then combine DAP and DAT to transform existing non-adaptive DNNs into a *Dimension-Adaptive Neural Architecture* (DANA) without altering other architectural aspects. Our solution does not need up-sampling or imputation, thus reduces unnecessary computations at inference time. Experimental results, on four benchmark datasets of human activity recognition, show that DANA prevents losses in classification accuracy of the state-of-the-art DNNs, under dynamic sensor availability and varying sampling rates.

Keywords—Deep Neural Networks, Time-Series Analysis, Sensor Data Processing, Adaptive Sampling, Sensor Selection.

1 INTRODUCTION

Health and wellness applications [1], [2], [3] exploit motion sensors embedded in mobile and wearable devices to infer body movements and temporal changes in the physiological state of the wearer [4], [5], [6], [7]. For example, static acceleration, that shows the magnitude and direction of to the earth's gravitational force, helps to recognize the wearer's posture; whereas dynamic acceleration, that shows changes in the motion velocity of the wearer, can be mapped to the wearer's different activities [8].

The time series generated by these motion sensors are processed over temporal windows and classified by deep neural networks (DNNs) [9], [10], [11], which mostly process sensor data with pre-defined, fixed dimensions [11], [12], [13], [14], [15], [16], [17], [18], and cannot reliably handle dynamic situations (*e.g.* when the sampling rate changes or some sensors are dropped), which are important for energy preservation [19], [20], privacy protection [21], [22] and fault tolerance [23], [24]. Moreover, DNNs are often trained on datasets collected from specific devices, but at the inference time they might be used in a wider set of devices, with different combinations of sensors and sampling rates [25].

Previous methods address either sensor selection [26], [27], [28], [29], [30], [31] or adaptive sampling rate [32], [33], [34], [35], [36]. A classical solution is to dedicate a classifier

for each feasible setting [37] or to perform multimodal fusion between predictions produced by multiple DNNs [38], [39]. The trade-off between classification accuracy and power consumption varies with changes in the sampling rate, the sensor streams used by the classifier, the type of the current activity, and the physical characteristics of the wearer [40]. Power-aware sensor selection may use a meta-classifier [26], or the prediction of future activities from the current one to deselect sensors that are not useful for future activities [27]. Alternatively, a graph model representing the correlation among sensors with a greedy approximation can be used for sensor selection [29], or a subset of sensors can be dynamically selected by minimizing an objective function based on classification accuracy and the number of sensors [31].

Defining an appropriate sampling rate that captures discerning frequency components for different activities, for example to minimize power consumption [19], is challenging [33] as the minimum required sampling rate varies across users, activities, and sensor position. Khan *et al.* [33] show that minimum sampling rate across activity recognition datasets varies between 22 and 63 Hz, for a 99% Kolmogorov-Smirnov similarity test [41]. It is therefore important to avoid aliasing to maintain the discernibility of activities characterized by higher frequencies [35], [36].

Yan *et al.* [40] propose to use a classifier with the highest sampling rate and then, after recognizing the current activity, switch to a lower sampling rate with another classifier and only monitor if the current activity changes. In order to lower power consumption, AdaSense [32] periodically detects changes in the current activity, by sampling data at higher frequencies, to check whether a lower sampling rate is suitable. To determine the best trade-off between power consumption and classification accuracy, Cheng *et al.* [34]

- * Corresponding author: m.malekzadeh@qmul.ac.uk
- Mohammad Malekzadeh, Richard G. Clegg, and Andrea Cavallaro are with School of Electronic Engineering and Computer Science, Queen Mary University of London. E-mails: m.malekzadeh@qmul.ac.uk, r.clegg@qmul.ac.uk, a.cavallaro@qmul.ac.uk.
- Hamed Haddadi is with Dyson School of Design Engineering, Imperial College London. E-mail: h.haddadi@imperial.ac.uk

find an optimal classification model as well as appropriate sampling rates using a continuous state Markov decision process that is only appropriate for training simple classifiers, such as softmax regression, and not applicable in training DNNs.

We introduce Dimension-Adaptive Neural Architecture (DANA) that, as a unified solution, is robust to variable sampling rates and sensor selection, and work on any combination of sensors that were considered at training time. Specifically, we introduce a dimension-adaptive pooling (DAP) layer that captures temporal correlations among consecutive samples and dynamically adapts to all feasible data dimensions. To enable DNNs that use DAP to generalize at inference time over the set of feasible dimensions, we propose a dimension-adaptive training (DAT) procedure, which incorporates dimension randomization and optimization with accumulated gradients. In each forward pass, DAT re-samples a batch of time windows to a new rate and may also randomly remove streams from some sensors. Then, gradients from several batches are accumulated before updating the parameters.

Combining DAP and DAT, we show how to transform existing DNNs into an adaptive architecture, while keeping the same size and accuracy, and improving the inference time. Beside allowing adaptive sampling rate and sensor selection in a unified solution, DANA also enables power-limited devices to take advantage of convolutional layers capability in reducing the performed computations according to the dimensions of the sampled data. Experimental results on four benchmark datasets show that DANA can maintain classification accuracy in dynamic situations where existing DNNs drop their accuracy and better generalizes to unseen environments. Code and data to reproduce results are publicly available at <https://github.com/mmalekzadeh/dana>.

The paper is organized as follows. Section 2 covers the background and related work. In Section 3, we elaborate on how a DAP layer works and in Section 4 we show how DNNs that use DAP can be efficiently trained using DAT. Finally, in Section 5 we evaluate DANA and compare it to non-adaptive DNNs and other baselines¹.

2 RELATED WORK

The architecture of a DNN is mainly defined by the type and number of the layers, and the way these layers are connected to each other [42]. The most common DNN architecture for sensor data classification is composed of a convolutional neural network (CNN) followed by a feedforward neural network (FNN) or a recurrent neural network (RNN) [10], [11], [12], [13], [14], [15], [16], [17], [18]. The main difference between FNNs and RNNs is that there are no feedback connections in an FNN such that outputs of a neuron is fed back into itself, whereas every neuron in an RNN includes a feedback connection. A CNN is inherently adaptive to input data of variable dimensions [43] and is mainly used for feature extraction for the downstream task [42]. Feeding such extracted features to an FNN or an RNN improves the

classification accuracy and provides a better generalization, compared to feeding raw sensor data [44]. However, FNNs only work on fixed-dimension input data, and RNNs only accept a fixed number of streams, thus making the combination of CNNs with FNNs/RNNs non-adaptive to the changes in input dimensions.

To address this limitation, a pre-processing stage can be added to the inference pipeline that up/down-samples data to a fixed rate or imputes dummy data to compensate for missing samples [45], but these solutions reduce classification accuracy and can raise some security challenges [46]. Alternatively, to turn deep architectures based on CNNs and FNNs/RNNs adaptive to changes in input-data dimensions, a preferable solution is to include an adaptive layer between the CNN and the FNN/RNN. A global pooling layer [47] takes the maximum or average over each filter map of the CNN's output to make a one dimensional vector whose length is equal to the number of the convolutional filter maps, and independent of the dimensions of these filter maps. The main drawback of global pooling is ignoring the inherent structure of the data, and we show that it causes accuracy loss.

To mitigate the shortcomings of global pooling in visual object recognition, spatial pyramid pooling (SPP) [48] runs pooling on a pyramid that is created by hierarchically dividing a feature map into equally sized segments. SPP is supported by a weight-sharing mechanism for training CNN-FNN architectures on different image resolutions, and is used for transfer learning: the CNN part trained on the source dataset can be used with another FNNs on the target dataset [49]. SPP has promising results in image processing [50], but is not applicable to CNN-RNN architectures where recurrent layers, such as LSTMs [51], need two-dimensional inputs that preserve the temporal correlation among consecutive samples and across different sensor streams. Therefore, global or pyramid layers are not directly applicable to RNNs, which are often preferred for time-series classification [52]. Moreover, given DNNs for multivariate sensor data, there is no way for existing pooling layers to make them adaptive to temporal changes in input layer dimensions without changes that increase or decrease the number of trainable parameters and consequently may affect the model's accuracy.

A DNN that can process variable input dimensions should also be trained to produce accurate outcomes with any feasible input dimensions. *Weight Averaging* [48] was proposed to build a single DNN by averaging the weights across multiple DNNs trained in parallel across different settings, which is also used in federated learning where the goal is to collaboratively train a shared model across different users [53]. Similarly in meta-learning the goal is to train a model across a large number of different tasks [54]. *Reptile* [55] is a meta-learning algorithm uses the average parameters of multiple DNNs, each trained on a different task, as input to the optimizer for updating the DNN's parameters, instead of directly using the gradients of the loss function.

Unlike existing adaptive pooling layers [47], [48], our proposed DAP layer considers the temporal correlations in data as well as the presence/absence of some of the sensors. This is particularly important as RNNs are more

1. For notation, we use lower-case *italic*, e.g. x , for single-valued variables; upper-case *italic*, e.g. X , for single-valued constants; standard **font**, e.g. \mathbf{X} , for vector, matrices, and tensors; and standard blackboard bold, e.g. \mathbb{X} , for unordered sets.

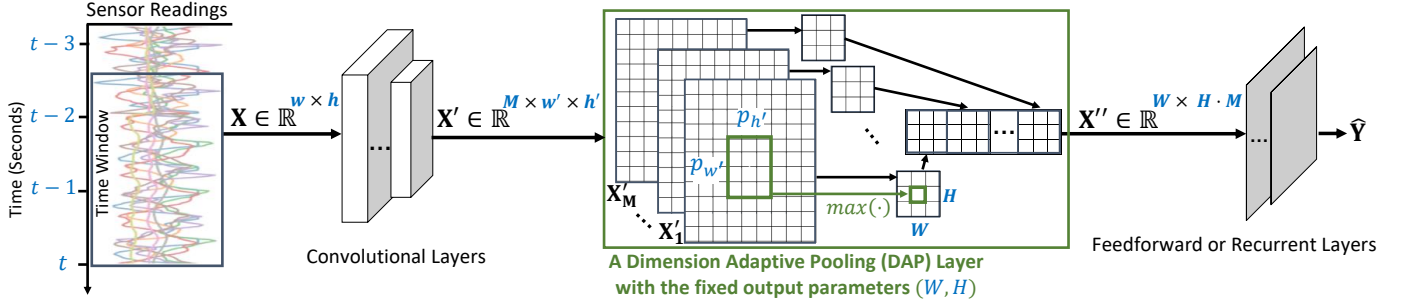


Fig. 1: A DAP layer enables a DNN performing classification on input data of variable dimensions. At time t , a window \mathbf{X} of dimensions $w \times h$ is produced. The number of *streams*, h , depends on the number of available 3-dimensional motion sensors, while the number of *samples*, w , per each stream depends on the current sampling rate (in Hz) and the length of time window (in seconds). For example, a 2.5-seconds time window of 50 Hz data generated by accelerometer, gyroscope, and magnetometer of a smartwatch has dimensions of $w = 125$ and $h = 9$. Convolutional layers process \mathbf{X} , then DAP is applied to the M outputs of the last convolutional layer, \mathbf{X}' . DAP uses an adaptive kernel of size $(p_w', p_{h'})$ that is calculated based on DAP's chosen parameters, (W, H) , and the dimensions of CNN's outputs, (w', h') . Finally, data of fixed dimensions, \mathbf{X}'' , is provided for the following feedforward or recurrent layers that are estimating a probability distribution, $\hat{\mathbf{Y}}$, over the possible outcomes. Note that, \times separates the size of each dimension while \cdot denotes product.

efficient in processing temporal data than FNNs [14], [15], [16]. Moreover, the proposed DAT resolves the need for weight sharing via training multiple DNNs, providing a faster and more accurate training algorithm, compared to the existing ones [48], [53], [55]. Finally, our solution resolves the need for training and deploying multiple DNNs to perform multimodal fusion [38], [39] which is particularly important for applications running mobile and wearable devices with limited power and processing resources.

3 DIMENSION-ADAPTIVE POOLING

We propose the DAP layer to handle situations where one or more sensors may dynamically be deselected at inference time. The flexibility of DAP aims not only to make DNNs adaptive to changes in the dimension of data, but also to allow efficiently training the DNN such that it provides reliable performance across several combinations of data dimensions.

Considering a multivariate time-series (see Figure 1), let \mathbf{X} be time window of dimensions $w \times h$ where w is the number of samples, which depends on the sampling rate and the length of time window, and h is the number of sensor streams. Specifically, motion sensors have three spatial axes (x, y, z) , thus $h = 3 \cdot s$, where s is the number of available sensors. Thus, if a sensor is not available, or deselected, then \mathbf{X} will have 3 less streams.

A DNN can cope with inputs of variable dimensions by using a convolutional layer as the input layer. A two-dimensional convolutional layer slides M fixed-sized *filters* across the input data, and computes dot products between each filter's entries and the data at the current position of the filter, resulting in M two-dimensional filter maps (\mathbf{X}' s in Figure 1). In a stack of convolutional layers, the dimensions of the CNN's output, $w' \times h'$, mainly depend on the dimensions of the input data², $w \times h$.

Typically, the CNN's outputs are reshaped into one-dimensional data of size $w' \cdot h' \cdot M$ for FNNs or two-dimensional data $w' \times h' \cdot M$ for RNNs. However, these typical DNNs can cope only with input data of fixed dimensions. One cannot simply use currently existing layers to make DNNs, which are proposed for processing sensor time-series, adaptive to the sampling rate and sensor selection without imposing any other architectural changes.

For instance, the single-dimensional data produced by SPP [48] is not appropriate for RNNs where the input must be provided in two dimensions: consecutive samples and parallel streams. DAP addresses the aforementioned limitations without enforcing assumptions on the desired DNN. DAP builds upon the global and pyramid pooling ideas and aims to map the outputs of dimensions $w' \times h' \times M$ into data consistent with the next FNN/RNN layer. The size of the pooling filters in DAP is not limited to be square, hence it generalizes existing adaptive layers [47], [48].

Algorithm 1 shows the functionality of DAP layer for DNNs processing motion sensor data³. Let (W, H) be the pre-specified hyper-parameters for pooling all the M feature maps into an output \mathbf{X}'' of single dimension of size $W \cdot H \cdot M$ (if the next layer is FNN) or two dimensions $W \times H \cdot M$ (if the next layer is RNN). DAP first calculates the pooling parameters $(p_w' = \lfloor \frac{w'}{W} \rfloor, p_{h'} = \lfloor \frac{h'}{H} \rfloor)$ for the received inputs. It then, for every segment of size $(p_w', p_{h'})$ on the received input, chooses the maximum value to create a the output which aims to be of fixed-dimensions (W, H) . For larger data dimensions, the pooling parameters adaptively cover a larger segment of the data and for smaller data dimensions they will shrink appropriately. Hence, DAP always produces an output of fixed dimensions.

As an example, consider a CNN-RNN and $s = 3$, $w' = 128$, $h' = 9$, $W = 16$, $H = 3$, $M = 32$. The maximum of every 8 consecutive samples among all 3 axes of each sensor will be chosen for the output, thus producing \mathbf{X}'' with dimensions

2. Design parameters such as the number of convolutional filters, M , size of the filters, the chosen padding mode, and the stride length of the filters are fixed at inference time.

3. $\lfloor \cdot \rfloor$ denotes floor, $\lceil \cdot \rceil$ denotes ceiling, and $\lceil \cdot \rceil$ denotes rounding to the nearest integer.

Algorithm 1 Dimension Adaptive Pooling.

```

1: Input:  $\mathbf{X}'$ : filter maps received from a CNN,  $(W, H)$ : the
   fixed output parameters.
2: Output:  $\mathbf{X}''$ : input to the next layer.
3:  $M, w', h' = \text{dimensions\_of}(\mathbf{X}')$ 
4:  $\mathbf{X}'' = \{\}$ 
5: for  $m = 1$  to  $M$  do
6:    $\mathbf{V} = \mathbf{X}'[m]$ 
7:    $\mathbf{Z} = \text{copy\_of}(\mathbf{V})$ 
8:    $a = \max(\lceil (H - h')/3 \rceil, 0)$ 
9:   for  $i = 1$  to  $a$  do
10:     $\mathbf{Z} = \text{concatenate\_vertically}(\mathbf{Z}, \mathbf{V})$ 
11:   end for
12:    $\mathbf{Z} = \mathbf{Z}[0 : w', 0 : \max(h', H)]$ 
13:    $p_{w'} = w'/W$ 
14:    $p_{h'} = h'/H$ 
15:    $\mathbf{Q} = \{\}$ 
16:   for  $i = 1$  to  $W$  do
17:     for  $j = 1$  to  $H$  do
18:        $r_1 = \lfloor i \cdot p_{w'} \rfloor$ 
19:        $r_2 = \lfloor (i + 1) \cdot p_{w'} \rfloor$ 
20:       if  $a=0$  then
21:          $c_1 = \lfloor j \cdot p_{h'} \rfloor$ 
22:          $c_2 = \lfloor (j + 1) \cdot p_{h'} \rfloor$ 
23:       else
24:          $c_1 = \lfloor j \cdot \lfloor (a + 1) \cdot p_{h'} \rfloor \rfloor$ 
25:          $c_2 = \lfloor (j + 1) \cdot \lfloor (a + 1) \cdot p_{h'} \rfloor \rfloor$ 
26:       end if
27:        $\mathbf{Q} = \text{append}(\mathbf{Q}, \max(\mathbf{Z}[r_1 : r_2, c_1 : c_2]))$ 
28:     end for
29:   end for
30:    $\mathbf{X}'' = \text{append}(\mathbf{X}'', \mathbf{Q})$ 
31: end for

```

$16 \times 3 \cdot 32$. If we deselect two sensors and choose a sampling rate half of the original, this means $w' = 64$ and $h' = 3$, then DAP adaptively keeps the output fixed, by choosing the maximum of every 4 consecutive samples of every single axis of the only available sensor.

The input of DAP has dimensions $w' \times h'$, which can be variable at training and inference time; whereas the output of DAP, \mathbf{X}'' , is fixed and includes $W \cdot H \cdot M$ values. The first inner loop in Algorithm 1 (lines 9-11) handles situations when one or more sensors are unavailable. Depending on the value of H , we may need to replicate some of the existing streams to satisfy fixed-sized outputs. For a DAP layer with $W = 16$, $H = 9$ and 3 sensors, the possible situations are as follows.

(1) All the sensors are available ($h' = 9$), thus $a = 0$ and the algorithm skips the loop (Lines 9-11).

(2) One sensor is unavailable ($h' = 6$), thus $a = 1$ and the loop fills the gap by *vertically concatenating* a copy of the data from available sensors to the second dimension of the input data. Therefore \mathbf{Z} will have $h' = 12$ streams and Line 12 truncates \mathbf{Z} on its second dimension to ensure that its second dimension satisfies $H = 9$.

(3) Two sensors are unavailable ($h' = 3$), thus $a = 2$ and the algorithm fills the gap by *vertically concatenating* a copy of the data from the only available sensor two times. So, we

Algorithm 2 Dimension Adaptive Training.

```

1: Input:  $\mathbb{D}$ : training datasets,  $\Theta$ : trainable parameters,
    $E$ : number of epochs,  $\mathbb{U}$ : a subset of all feasible dimensions,
    $B$ : number of batches used in each optimization round,  $K$ : size of each batch.
2: Output:  $\Theta$ : optimized parameters.
3: for  $e = 1$  to  $E$  do
4:   while not feeding the DNN all data in  $\mathbb{D}$  do
5:      $\mathcal{G} = 0$ 
6:     for  $b = 1$  to  $B$  do
7:        $\mathbb{X} = \text{generate\_random\_batch}(\mathbb{D}, K)$ 
8:        $\mathbb{X} = \text{dimension\_randomization}(\mathbb{X}, R)$ 
9:        $\hat{\mathbb{Y}} = \text{forward\_pass}(\Theta, \mathbb{X})$ 
10:       $\mathcal{G} = \mathcal{G} + \text{Gradients}(\text{Loss}(\mathbb{Y}, \hat{\mathbb{Y}}))$ 
11:     end for
12:      $\Theta = \text{optimizer}(\Theta, \mathcal{G})$ 
13:   end while
14: end for

```

will again satisfy $H = 9$.

Note that Line 12 guarantees that, in case of concatenating data to \mathbf{Z} , the number of streams in data never exceeds H , and it has a neutral effect when $h' = H$. The next two loops, in Lines 16-29, perform the pooling operation over the consecutive segments of \mathbf{Z} .

Following our example, in each iteration we consider a segment of data including w'/W samples and h'/H streams. For example, if $w' = 96$ then the maximum of every 6 consecutive samples of each sensor stream (e.g. the accelerometer's x axis) is calculated and appended to \mathbf{Q} (Line 27). If we only change H to 3, instead of 9, a will be zero, thus no concatenation happens. On the other hand, every segment of data includes $6 \cdot 3 = 18$, $6 \cdot 2 = 12$, or $6 \cdot 1 = 6$ samples if all three, two, or only one sensor(s) are available, respectively. Therefore, DAP adaptively changes the size of pooling segments to ensure that the output dimensions are fixed. Also note that, in Lines 16-29, the first loop runs on the first dimension W and the second loop on the second dimension H : this order preserves the temporal correlation among consecutive samples, which is necessary for DNNs that use recurrent layers.

4 DIMENSION ADAPTIVE TRAINING

Although a DNN using DAP can accept input with any dimensions, it should properly trained for being adaptive to changes, otherwise its performance will be poor. The *multi-size training* procedure [48] for images trains in parallel two DNNs with different dimensions but with shared weights. This multi-size training is problematic with sensor data because of the large variety of possible training situations. For example, 10 sampling rates (e.g. 5, 10, 15, ..., 50 in Hz) and the 7 possible combinations of 3 sensors leads to 70 DNNs to train.

To overcome this challenge and provide a reasonable, converging training strategy, we propose dimension adaptive training (DAT). In DAT, we train a single DNN and therefore there is neither a need for weight sharing nor for choosing a specific set of data dimensions. DAT comprises of two main ideas: *dimension randomization* and *optimization with*

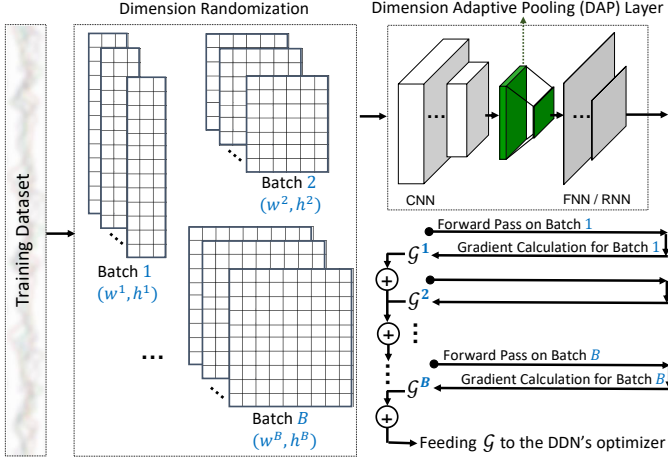


Fig. 2: Overview of each iteration in DAT. B batches of time windows are randomly generated from a training dataset. Samples within each batch have the same dimension while samples among batches have different dimensions. All time windows in each batch are transformed into the same randomly chosen dimensions $w^b \times h^b$. Every batch is iteratively fed into DNN and the corresponding gradients with respect to the current loss value are accumulated into \mathcal{G} . Finally, the parameters of the DNN are updated based on \mathcal{G} .

accumulated gradients (Figure 2). The DAT process works by training the DNN on input data of several randomly selected dimensions. For efficiency, the data is processed in batches of input data with the same dimension. The details of DAT are shown in Algorithm 2.

Each round of optimization includes two steps. First, a random batch, \mathbb{X} , of K time windows of the highest available sampling rate is generated from the dataset. For batch number b , the available sensors are chosen randomly and a random sampling rate is chosen with data downsampled using bilinear interpolation. All the time windows in batch b have the same dimensions⁴ $w_b \times h_b \in \mathbb{U}$.

Considering an example where the possible sampling rates range from 6 Hz to 50 Hz, instead of considering all the 46 possible cases, we only choose a subset \mathbb{U} , for instance including 8 equally distanced sampling rate $\{6, 12, 18, 25, 31, 37, 43, 50\}$ (in Hz). In the epoch e , $\text{dimension_randomization}()$ in Line 8 randomly and uniformly chooses, for instance $B = 4$ of this 8 sampling rates without replacement. Second, a forward pass is performed on batch b giving a vector of predictions, $\hat{\mathbb{Y}}$. we calculate the average loss value (e.g. categorical cross-entropy) of the predictions compared with the true labels, \mathbb{Y} , and its gradients, corresponding to the Θ , is accumulated into \mathcal{G} . These two stages are repeated B times, then using the accumulated gradients, \mathcal{G} , the parameters the DNN, Θ , are updated at once.

As DNNs tend to forget previously learned information upon learning from new data, updating Θ immediately after computing losses for each batch of data cause catastrophic forgetting [56], in which the DNN may repeatedly forget how to perform classification on the previously trained

4. Note that, the key point of efficiently training DNNs on GPUs is in eliminating loops by matrix multiplications that forces all samples in each batch, b , to have the same dimensions in a forward pass.

TABLE 1: Details of the four datasets used in the validation. For all datasets, the original sampling rate is 50 Hz.

Dataset	Characteristics		
	Sensors	Activity Classes	Users
UCI-HAR [59]	Accelerometer Gyroscope	{Sit, Stand, Walk, Lie Stairs-Down, Stairs-Up}	30
MobiAct [60]		{Sit, Stand, Walk, Jog, Stairs-Down, Stairs-Up}	61
MotionSense [61]			24
UTwente [62]	Accelerometer Gyroscope Magnetometer	{Sit, Stand, Walk, Jog, Bike, Smoke, Drink, Eat, Talk, Type, Write, Stairs-Down, Stairs-Up}	10

dimensions. The combination of dimension randomization and gradient accumulation not only helps DAT to prevent catastrophic forgetting but also to converge faster.

It is worth noting that the gradient accumulation in DAT is similar but a different concept than the typical method of keeping track of gradient *momentum* in stochastic gradient descent [57]. In a momentum-based optimization, a scaled version of the gradients used in the previous round is added to the gradients of the current round. Thus, at each round, the DNN's parameters are updated based on the current gradients and a history of the past gradients. On the other hand, DAT is a procedure for computing the required gradients in a single round, hence we can use DAT and a momentum-based optimization, such as Adam [58], together.

5 EVALUATION

We evaluate DANA on four public datasets of human activity recognition: UCI-HAR [59], UTwente [62], MobiAct [60], MotionSense [61]. We show how to transform three state-of-the-art CNN-FNN/RNN architectures for sensor-based human activity recognition [12], [13], [14] into a DANA, and discuss how DAP works with and without using DAT. We also evaluate the advantages of DANA at training time, compared with three other training procedures: *standard*, *weight averaging*, and *Reptile*, and at the inference time compared with two alternatives baselines: *imputation* and *resampling* with and without *data augmentation*. Finally, we perform a cross datasets experiment to show the generalization of DANA.

5.1 Datasets

UCI-HAR [59] is a widely used dataset [12], [13], [14], [15] of 30 users performing 6 activities. Accelerometer and gyroscope data were collected by a smartphone worn on the waist. Data from 21 users are used for training and that of the other 9 users for testing purposes [59].

UTwente [62] includes data of 10 users performing 13 activities. We use accelerometer, gyroscope, and magnetometer data collected from the device on the (right) wrist. We divide the dataset into 80% training and 20% validation.

MobiAct [60] and **MotionSense** [61] include accelerometer and gyroscope data from 61 and 24 users, respectively, with a smartphone in the pocket of the trousers. We use the data from the 6 activities in common among the two datasets. In the MobiAct dataset, for each activity, we keep 2/3 of

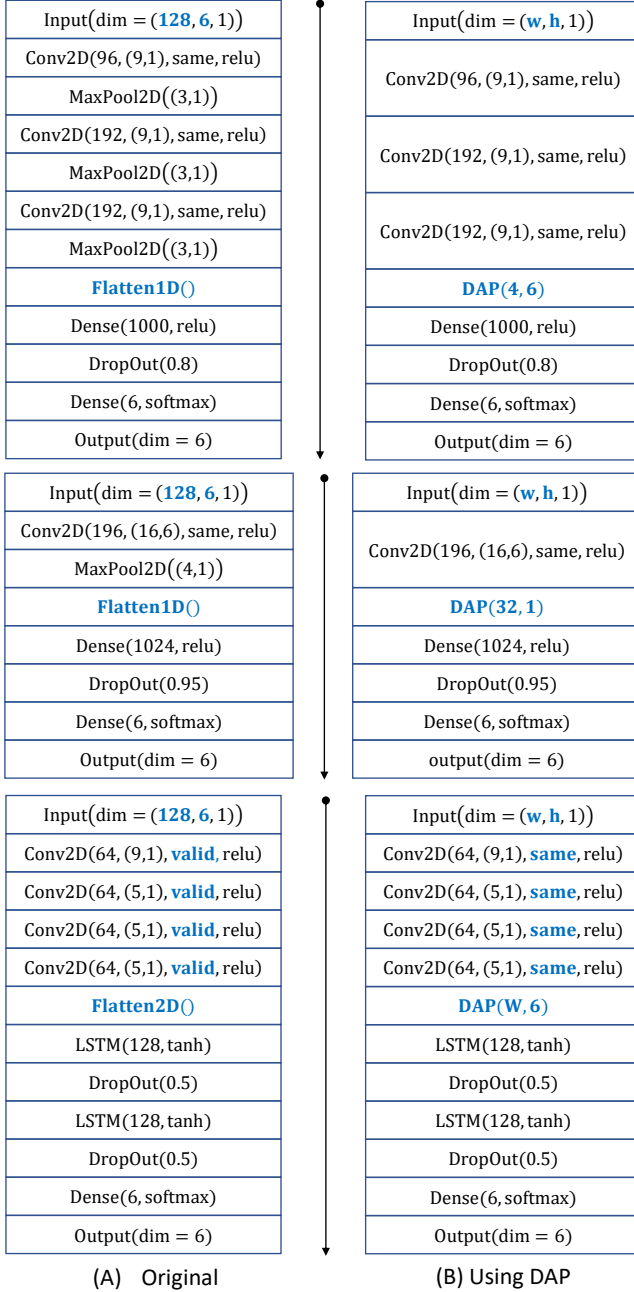


Fig. 3: The original (left) DNNs proposed by [12] (top), [13] (middle), and [14] (bottom) versus their DANA version (right). The differences between each pair of DNNs are shown in **blue bold** font. We use the TensorFlow [63] naming conventions.

trials for training and 1/3 of them for validation [61]. We use the entire MotionSense dataset for test purposes and do not use it at the training.

For all experiments, we use a time window $T = 2.56$ seconds (i.e. a maximum of 128 samples per window) [12], [13], [14]. Table 1 shows the details of the datasets, including the activity classes.

5.2 Transforming a DNN into DANA

Figure 3 shows the original architectures proposed in the related work [12], [13], [14] and our modified ver-

TABLE 2: Classification accuracy of three benchmark DNNs on UCI-HAR, the original non-adaptive model, versus the corresponding adaptive model with a DAP layer.

Architecture (Model Size)	DNN [(W, H)]	Setting	Accuracy (%)	
			Mean±STD	Maximum
CNN-FNN (5,114,014)	[12]	<i>validate</i>	93.85±.49	94.51
		<i>test</i>	91.92±.97	93.14
	with DAP(4,6)	<i>validate</i>	93.73±.84	95.39
		<i>test</i>	91.88±1.1	93.04
CNN-FNN (6,448,714)	[13]	<i>validate</i>	93.80±.59	94.78
		<i>test</i>	92.75±.73	94.02
	with DAP(32,1)	<i>validate</i>	93.89±.41	94.57
		<i>test</i>	92.57±.60	93.65
	[14]	<i>validate</i>	94.13±.53	95.25
		<i>test</i>	91.66±1.3	93.45
	with DAP(4,6)	<i>validate</i>	94.69±.31	95.32
		<i>test</i>	94.07±.39	94.77
CNN-RNN (457,030)	with DAP(8,6)	<i>validate</i>	94.82±.34	95.32
		<i>test</i>	93.47±.81	94.33
	with DAP(16,6)	<i>validate</i>	94.69±.48	95.18
		<i>test</i>	93.19±.59	94.02
	with DAP(32,6)	<i>validate</i>	94.74±.33	95.32
		<i>test</i>	93.23±.92	94.70

sion using DAP. A 2D convolutional layer is shown by $\text{Conv2D}(n, (k_1, k_2), \text{padding}, \text{activation})$ where n is the number of neurons, (k_1, k_2) is the size of the 2D kernel used by each neuron; if *padding* is *same*, the output and the input of the layer have the same dimensions, otherwise if it is *valid* then the output has $k_1 - 1$ and $k_2 - 1$ values fewer than the number of inputs in the first and second dimensions, respectively; *activation* shows the nonlinear activation function applied to the output of the layer; $\text{Dense}(n, \text{activation})$ shows a fully-connected feedforward layer; $\text{LSTM}(n, \text{activation})$ shows a recurrent LSTM [51] layer; $\text{MaxPool2D}((p_1, p_2))$ shows a 2D maximum pooling layer that outputs the maximum value of each window including $p_1 \cdot p_2$ data points; $\text{Dropout}(q)$ applies Dropout [64] with probability q that randomly sets the output of a neuron to 0 during each forward pass in training time; $\text{Flatten}()$ reshapes its inputs into 1D or 2D outputs.

To transform a non-adaptive DNN into a DANA, we only use a single DAP layer, instead of “maximum pooling” layers, with an appropriate pooling parameters (W, H) , and instead of “valid” padding we use “same” padding. Thus, we can keep the total number of the trainable layers and parameters exactly the same as the original DNN.

5.3 Original DNNs versus Their DANA Version

To ensure the comparison is fair among all DNNs, we use the same number of epochs (1,000), early stopping patience (100 epochs), and batch size (128). We also use the same optimizer as reported in the corresponding works: for the models with FNN, Adam [58], and for the models with RNN, RMSProp [65]. We run each model 10 times and report the mean and standard deviation for classification accuracy.

Table 2 compares the classification accuracy for each DNN architecture with that architecture using DAP instead of their standard maximum pooling. Although we set (W, H) such that having the same model size as the original DNN; it is possible to choose any other values getting a larger or smaller size DNN. Here, two settings are considered for evaluations. (i) *Validate*: where the whole training dataset

TABLE 3: Classification accuracy (%) of three benchmark DNNs on UTwente, the original non-adaptive model versus the corresponding adaptive model using a DAP layer.

DNN	Size	Ref.	Accuracy	
			Mean \pm STD	Maximum
CNN-FNN	7,425,021	[12]	59.20 \pm 9.6	76.99
	12,878,417	[13]	78.85 \pm 6.2	88.01
		[14]	93.68 \pm .36	94.55
CNN-RNN	556,237	with DAP(8,9)	94.35 \pm .37	95.16
		with DAP(16,9)	94.64 \pm .40	95.40

is used for training, and test dataset is used for validation. Thus, each DNN is trained on the training dataset and the validation dataset is used to check the accuracy of the model after each epoch. This is the setting that is used by other works re-implemented [12], [13]. (ii) *Test*: where 10% of the training dataset is randomly chosen as the validation set and the rest of 90% is used as the training set. Here, the test dataset is used to evaluate the best trained DNN on the validation set.

Table 2 shows that for all three architectures the classification accuracy of the adaptive version is either slightly improved or almost the same as the original DNN, in both *validate* and *test* setting. This suggests that the DAP layer does not lead to a loss in accuracy while providing the desirable adaptivity. The CNN-RNN model has 10 times fewer parameters than the FNN but has a better classification accuracy. The CNN-RNN with DAP significantly improves accuracy in the *test* setting, thus suggesting that DAP helps the model to better generalize to the test data. RNNs are also flexible on their first dimension, which is the number of samples per stream. Thus, unlike FNNs, we can use DAP layers having different pooling parameters for the first dimension while keeping the rest of the architecture the same. Changing the pooling parameters leads to slightly different accuracies, which can be used as part of a fine-tuning pipeline for DNN models but would not be possible with FNNs.

To see the performance of the DNNs and DANA on another dataset, we evaluate existing DNNs (without fine-tuning) on UTwente, which is a different dataset from those datasets used in the original papers of the implemented DNNs. Table 3 shows that the CNN-RNN architecture has better generalization than the other two CNN-FNN architectures. The model using DAP maintains a comparable accuracy, even slightly better.

We see that transforming a DNN into DANA does not change the trainable parameters of the DNN, whereas using other global pooling or SPP layers would require a change in the size of the FNN/RNN layers and consequently the number of trainable parameters of the original DNN. As an experiment, to measure the effect of using the global average pooling layer [47], we run a similar experiment on CNN-RNN [14] with UCI-HAR. The model size is reduced from 457K to 293K, but also the classification accuracy (%) reduced from 94.13 \pm .53 to 78.6 \pm .81.

It should be noted that this experiment only aims to show that using a DAT layer does not degrade the accuracy, and not to show that using a DAT layer we can achieve better accuracy in a fixed-dimensions scenario. As we show in other experiments, the main advantage of DANA is keeping high accuracy in variable-dimensions scenarios. As the *validate*

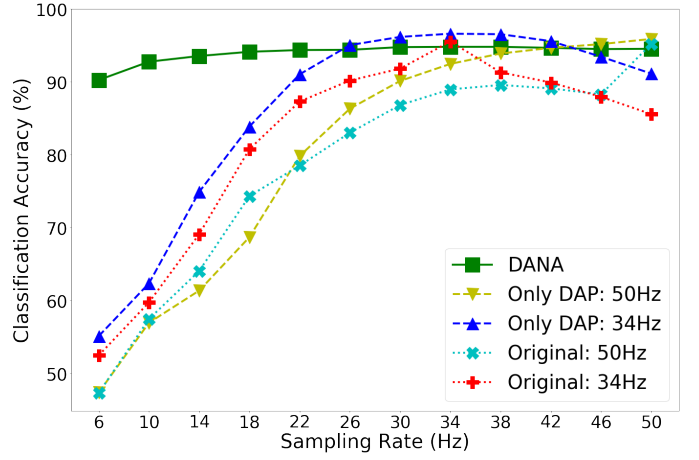


Fig. 4: Classification accuracy of CNN-RNN [14] on UCI-HAR for different sampling rates.

setting is what is considered in other works [12], [13], where they report the *best accuracy* that corresponding DNN can achieve on the dataset, for the rest of the experiment we use the *validate* setting for fair comparisons. Note that as we do not tune any hyper-parameters and do not change the size of trainable parameters in all DNNs, similar relative results are achieved in the *test* setting. But, unlike the *validate* setting which has only one instance (*i.e.* a training set and a validation set), the *test* setting could be biased because there are many possible instances depending on the randomly chosen 10% validation set.

5.4 Changes in Sampling Rate and Sensor Availability

Figure 4 compares the original and DANA version of the DNN proposed by [14], as CNN-RNN performs better. First, using the original DNN, the model can only be trained and validated on data of fixed dimensions. To see how the original model performs if we change the sampling rate, we keep the weights and parameters of the original model and use them on a version using DAP (lines with a cyan cross and red plus). Second, we have a DNN version that only uses DAP during the training but only trained on a fixed sampling rate (lines with yellow and blue triangles). Finally, we have the DANA version (the line with green square) which not only uses DAP, but it also uses DAT with $B = 4$ and $\mathbb{U} = \{6, 12, 18, 25, 31, 37, 43, 50\}$ (in Hz).

Although DANA version slightly reduce the accuracy on the specific sampling rates the other DNN versions were trained on (34Hz and 50Hz), it considerably outperforms the other DNN versions across the whole range of sampling rates, where the accuracy of other DNNs drops quickly when moving away from their pre-defined setting. Because the best accuracy of DANA occurs at 34 Hz, for this reason, we trained other DNNs on this specific sampling rate, thus suggesting that DAT is consistent in its performance while being adaptive.

To see the effect of sensor selection, Figure 5 shows the replication of previous experiment (in Figure 4) in different sensor-selection scenarios. Here, DANA is trained to account for the possibility of deselecting (or missing) sensors, and the other lines are the same as in Figure 4 where the training only

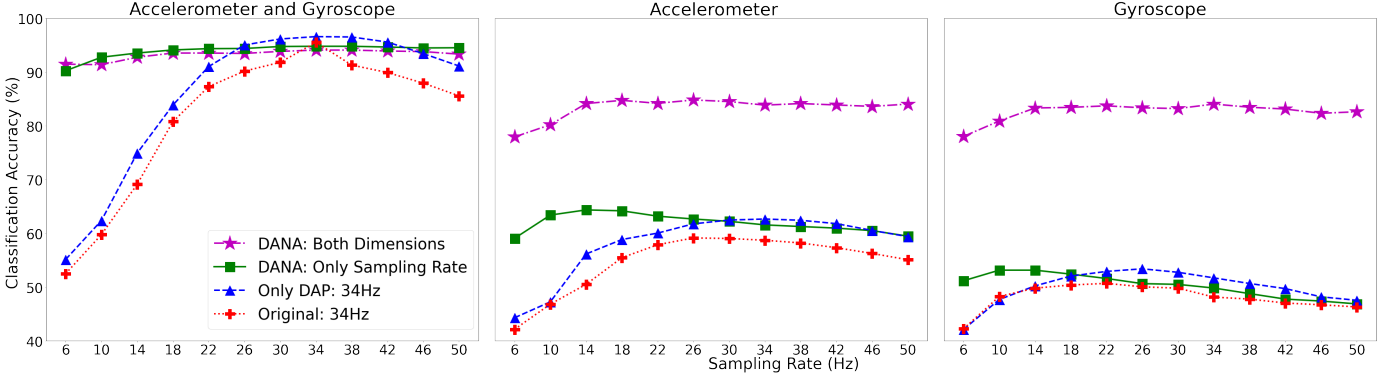


Fig. 5: Classification accuracy of CNN-RNN [14] on UCI-HAR with variable sensors.

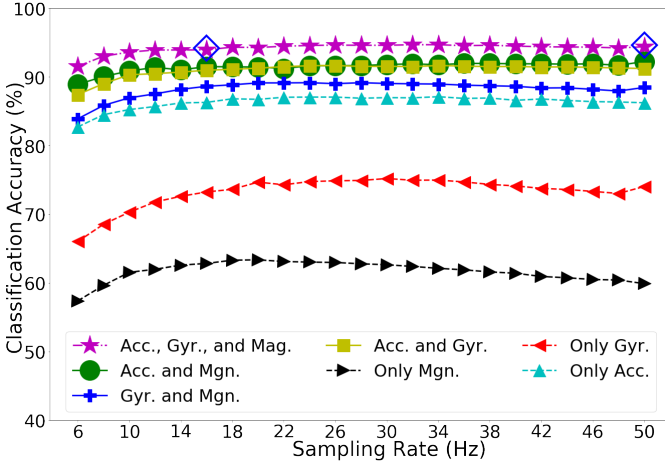


Fig. 6: Classification accuracy on UTWente with the DANA version of the CNN+RNN proposed by [14]. The two points shown by \diamond at 16 Hz and 50 Hz shows the accuracy of the original DNN when trained on these fixed sampling rates.

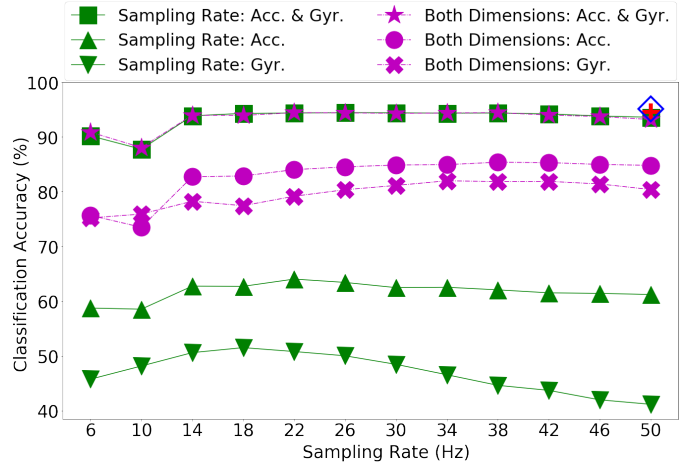


Fig. 7: Classification accuracy on UCI-HAR using a CNN-FNN [12]. The data points $+$ and \diamond at 50 Hz refer to Table 2 accuracies.

consider sampling rate selection and does not account for sensor selection. During training with DAT, the probability of deselecting each sensor is 25%. Therefore, 50% of the times, DANA is trained on both sensors, and 50% of the time with one of accelerometer or gyroscope. The values of B and U are the same as Figure 4.

Figure 5 (left) shows that the adaptivity to the sensor selection is not associated to a large penalty when all sensors are present. Figure 5 (middle) shows that when the gyroscope is deselected, DANA maintains its accuracy around 85% while the accuracy of other DNNs falls rapidly to around 60%. Similarly, Figure 5 (right) shows that when the accelerometer is deselected the accuracy for DANA remains around 85% while other techniques fall to 50% or less. It is interesting that while for other DNNs deselecting accelerometer data causes more accuracy loss than deselecting gyroscope, the type of the deselected sensor has a reduced effect on DANA.

In Figure 6 we make the CNN-RNN model adaptive to both sampling rate and sensor availability using DAP and DAT on UTWente, and we achieve a similar accuracy to the original model. Note that, while original DNNs are not reliable when the data dimensions change, DANA provides at least 55% accuracy across $7 \cdot 45 = 315$ feasible data

dimensions.

Figure 7 compares the accuracy for different versions of a CNN-FNN proposed by [12]. The accuracy of DANA, trained on both variable sampling rates and variable sensors, remains high for a variety of sampling rates. When one of two sensors is deselected, the accuracy loss is much smaller than the one obtained when training only on variable sampling rates, with fixed sensors. The accuracy loss for this generalization is small when compared with the single points that show the situations where the DNN is only trained on a fixed sampling rate with all sensors present without and with DAP, respectively.

5.5 A Cross-Dataset Experiment

We train three versions of the CNN-RNN proposed in [14] on MobiAct and test them on MotionSense. We follow two settings: *normalized*, where we normalize the MotionSense data to mean zero and unit standard deviation, and *pseudo-normalized*, where we use the MobiAct statistics to normalize the MotionSense data to mean zero and unit standard deviation. The latter is standard practice as, when streaming data, the mean and standard deviation are not known in advance.

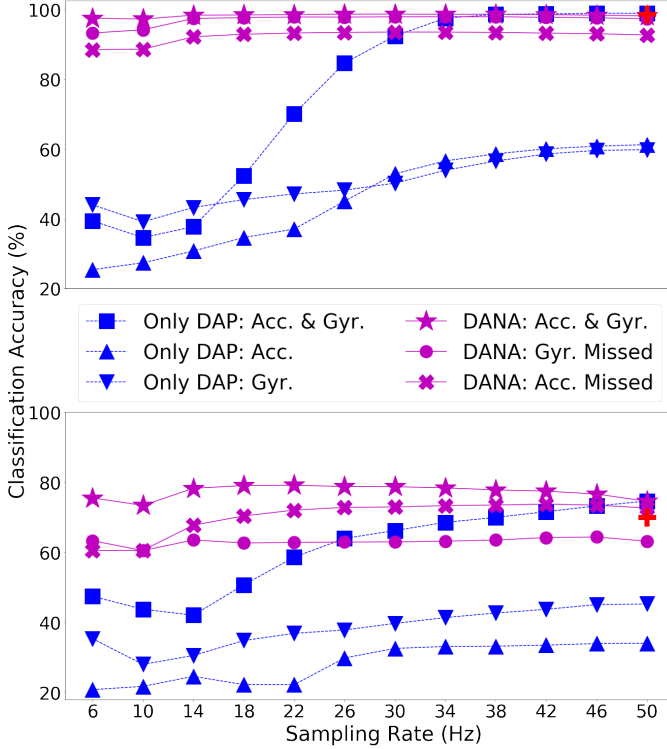


Fig. 8: Classification accuracy of a CNN+RNN [14] trained on MobiAct [60] and tested on MotionSense [61]. The single data point shown by + at 50 Hz refers to the accuracy achieved with the original DNN in Table 4.

Table 4 shows that DANA generalizes better on the test dataset, in terms of accuracy, by about 5 percentage points. All three models have the same number of parameters and were trained under the same training setting. This result confirms that for the corresponding datasets, making a DNN adaptive (using DAT) helps to achieve a more accurate model in an unseen environment⁵. Although the DANA version has a slightly smaller accuracy than the one using only DAP, DANA is the only reliable model when the dimensions of the input data change (see Figure 8). Thus, while DANA shows a bit smaller accuracy than original DNN on MobiAct, this will considerably payoff when DANA is used in dynamic settings which we have shown in the results of the previous experiments.

5.6 Comparison with Baselines

A alternative baseline to DANA is to take the original model and every time the sampling rate is changed, we fix the problem by re-sampling data to the original sampling rate, and if some sensors are missing or deselected, we impute dummy data, *e.g.* zeros. Another baseline is to use an *augmented* training dataset by making a copy of the data for every possible combination of sensors availability. For example, with 3 sensors, we build 6 other samples for each sample time-window in the training dataset, one for each

5. MobiAct was collected with a Samsung Galaxy S3 in the right or left pocket of the trousers. MotionSense was collected with an iPhone 6s in the front, right pocket of their trousers.

TABLE 4: Accuracy (%) of CNN-RNN architecture proposed in [14] trained on the MobiAct training dataset and validated on the MobiAct and MotionSense test datasets.

DNN	MobiAct	MotionSense	
		Normalized	Pseudo-Normalized
Original	98.64	69.87	44.16
Only DAP	98.91	74.65	49.65
DANA	98.18	74.60	47.97

possible setting. Hence, the training time for the *augmented* case is 7 times the training time for the original and DANA.

Figure 9 and 10 compares DANA with these baselines. We see that DANA can train a single model that outperforms the original model across all 56 settings, and also outperforms the augmented case for lower sampling rates (while remaining competitive for larger sampling rates). Note that the augmented baseline needs longer training time and also does not reduce the computations when sampling rate changes or some sensors are unavailable or deselected. These results show that DANA can capture the correlation, or information redundancy, among different sensor streams. For example, when the original models miss a sensor or two, their accuracy considerably falls, because they are not able to substitute the missed information using the available ones. But DANA keeps the accuracy at the same level of the augmented one, while it does not need to endure the difficulties of the augmented one at the training and inference time.

5.7 Comparison with other Training Approaches

We explore the impact of the value of the training hyperparameter B on the accuracy. Figure 11 shows, for both CNN-FNN and CNN-RNN, the classification accuracy is comparable for RNN for $B \geq 4$ (whereas FNN cannot be trained with these values), and in general it suggests to set a $B \geq 5$.

Table 5 shows that DAT either outperforms or achieves comparable accuracy to other methods in several settings, and is always faster in training. The training approaches we compare with are *Standard*, the typical training procedure that includes a forward pass on a batch of data to calculate loss value, following with a backward pass to update model parameters based on the gradients; *WeightAvg* [48], [53], when each of the B copies of the model is trained on a dedicated batch of data using the *Standard* approach, and then the average parameter values of updated B copies will be used to update the central model; and *Reptile* [55], which performs the same procedure as *WeightAvg*, except the last step when the average parameters of B copies, each trained on a different batch of data, is fed to the chosen DNN optimizer, instead of the typical gradients of the loss function, to update the central model. The value of B is fixed to 5 for all experiments in the Table 5. The *time* shows the average training time per each iteration over the whole training dataset (*i.e.* one epoch). Note that, DAT is not sensitive to the chosen optimizer, or dataset, or DNN architecture. Also, Reptile works with Adam (that is mentioned in the

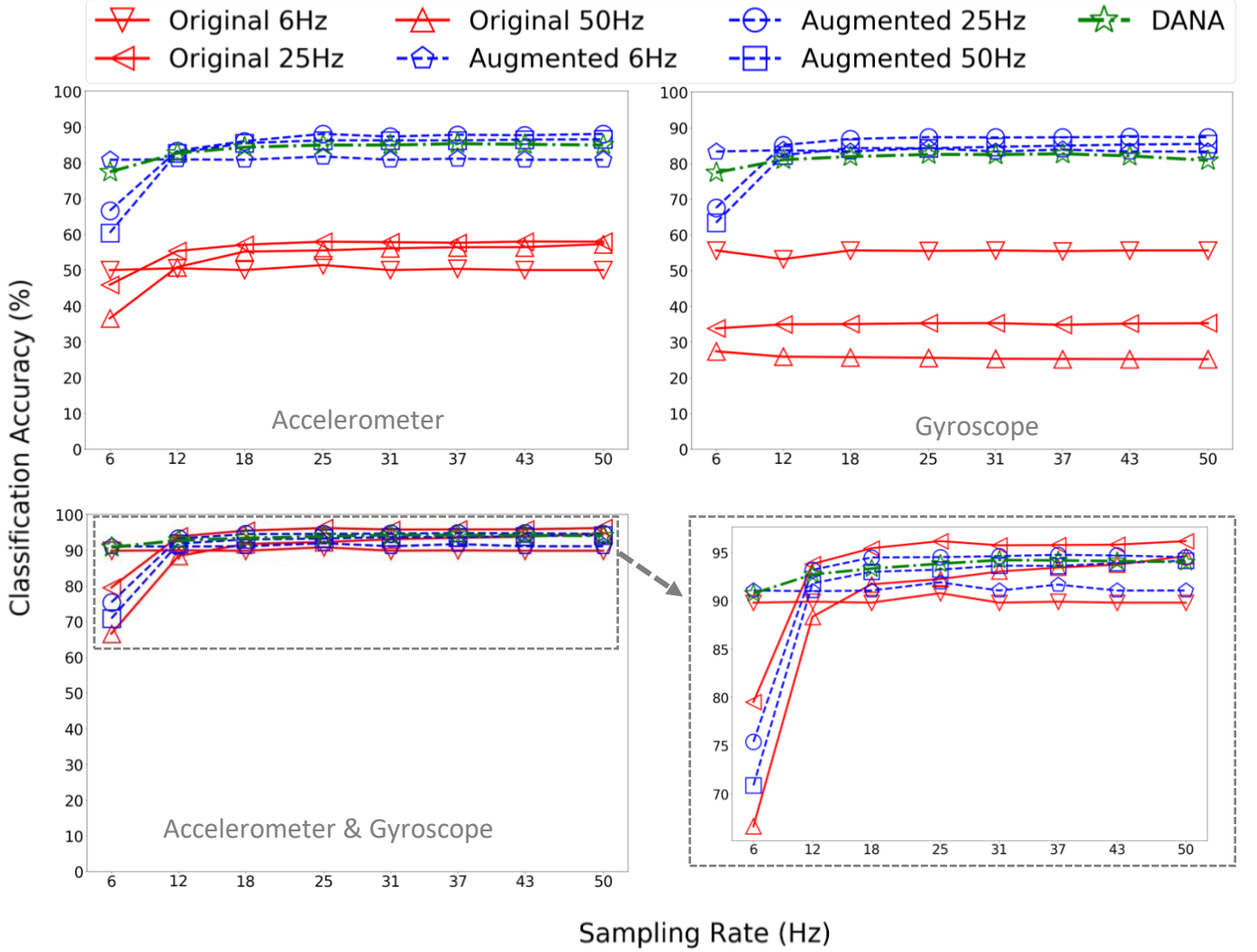


Fig. 9: Comparing baselines with DANA on UCI-HAR with CNN-RNN [14].

original paper [55]), but it cannot be useful with the RMSProp optimizer.

6 DISCUSSION

While we believe that DANA presents a unified solution to the problem of adaptive sensor and sampling rate selection, it also opens doors to some new challenges and research directions.

First, Unlike datasets of other data types, such as images or texts, the majority of public datasets of motion-sensor data do not simultaneously satisfy the requirements of abundance and variety of activities, users, devices, and number of sensors. Collecting, or getting access to, a larger dataset can help to evaluate DANA in more experimental scenarios.

Second, the focus and evaluation of DANA has been on motion sensor data. It might be helpful to apply DANA to other types of temporal data, such as audio streams or other types of sensors that have different data characteristics. This needs optimizing the code of the proposed DAP layer for other data types.

Third, measuring the impact of DANA in saving power consumption, when running on a wearable on mobile device,

and the required interplay between the operating system of the user's device is an important direction. DANA has application for situations where users want to control applications' permissions over sensors, which also require research in other aspects of such human-computer interactions.

Finally, to cover the whole range of possible data dimensions at the inference time, we randomly cover a subset of the possible situations at each round of training the DANA. One can study the behavior of this randomized selection alongside the DAT procedure to see if it is possible to provide a more theoretical analysis of the convergence of such training approaches.

7 CONCLUSION

We presented DANA, a solution to make deep neural networks adaptive to temporal changes in the dimensions of the input data to cope with adaptive sampling and sensor selection. DANA provides a single trained model that retains high classification accuracy across a range of settings, thus avoiding the need for a separate classifier for each setting at inference time. DANA imposes no limitations on the type of DNN and is flexible in shaping the DNNs without

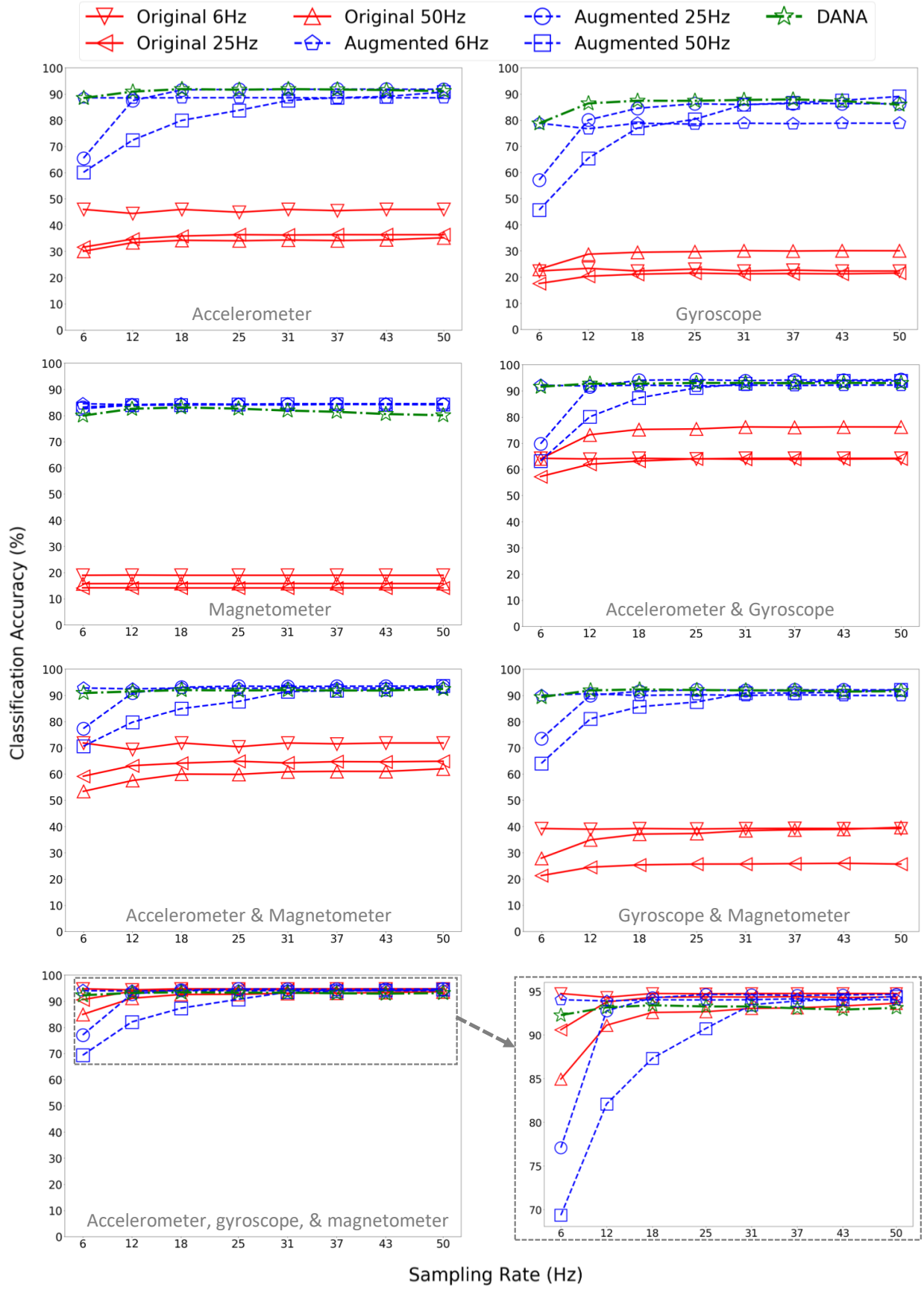


Fig. 10: Comparison of baselines and DANA with CNN-RNN on UTwente [14].

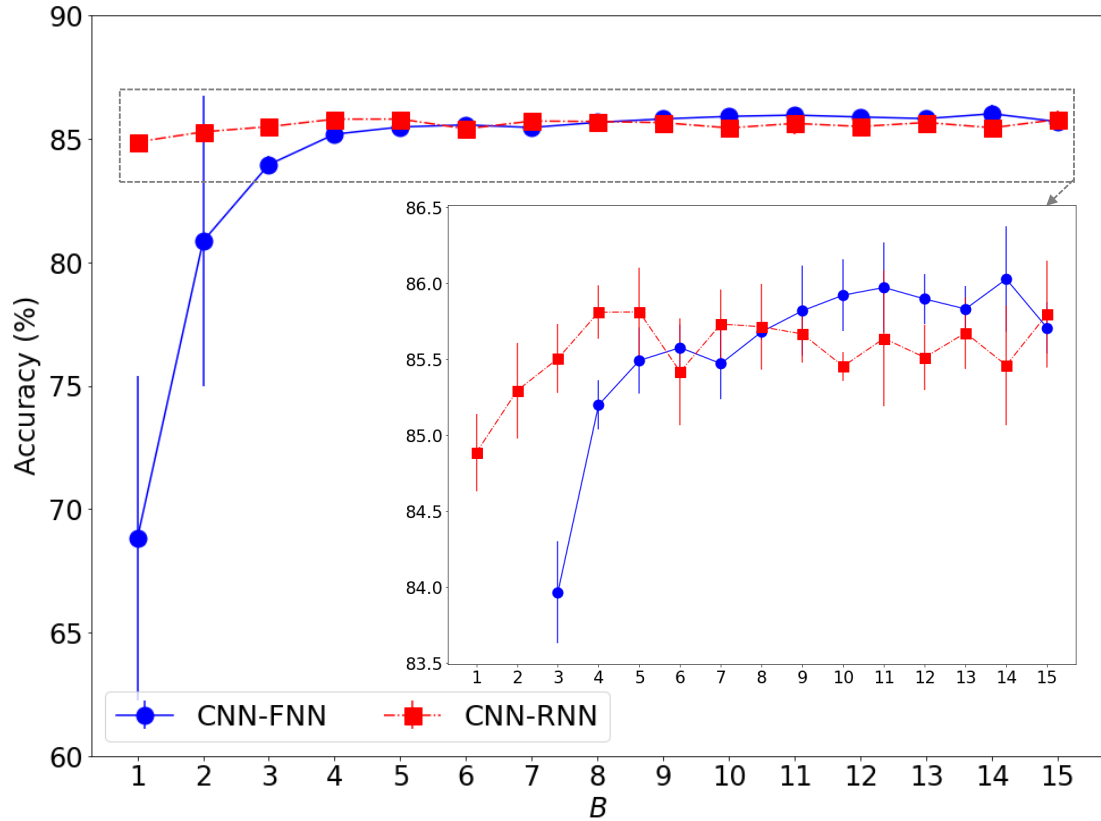


Fig. 11: Effect of the size of resampling batches B on UCI-HAR with CNN-RNN [14]. Each point is the average and each segment shows the standard deviation for 5 runs.

TABLE 5: Comparison of different training methods for turning a DNN adaptive to changes in the input data dimensions.

Dataset DNN Model Optimizer	UCI-HAR [59]						UTwente [62]	
	CNN+FNN [12] Adam		CNN+RNN [14] RMSProp		Adam		CNN+RNN [14] Adam	
Method	Accuracy (%)	Time (s)	Accuracy (%)	Time (s)	Accuracy (%)	Time (s)	Accuracy (%)	Time (s)
Standard	69.94±6.08	4.24±.29	86.21±.11	6.03±.17	86.98±.21	5.55±.15	87.02±.51	14.24±.44
WeightAvg	85.90±.25	5.63±.13	86.61±.19	6.54±.10	87.02±.21	6.07±.14	88.14±.99	15.03±.45
Reptile	85.73±.25	5.50±.11	15.91±2.25	6.23±.10	86.87±.26	5.96±.19	87.87±.74	15.01±.43
DAT (Ours)	85.74±.20	3.68±.08	87.12±.13	5.58±.15	87.50±.11	5.43±.15	88.91±.59	13.30±.57

adding or removing trainable parameters. We showed that our proposed approach outperforms the state of the art over a range of sampling rates and retains accuracy when some sensors are unavailable at inference time. For instance, on a dataset of 3 sensors and 13 activities, DANA keeps classification accuracy similar to the original DNN in a range of 6Hz to 50Hz and its accuracy only falls from 95% to around 90% and 85% in case of missing one or two of the three sensors, respectively, while the original DNN cannot handle these changes, or achieve at most 75% and 55% accuracy with resampling and imputation preprocessing.

ACKNOWLEDGMENT

The work was supported by the Life Sciences Institute at Queen Mary University of London.

REFERENCES

- [1] Y. Nam, Y. Kim, and J. Lee, "Sleep monitoring based on a tri-axial accelerometer and a pressure sensor," *Sensors*, vol. 16, no. 5, p. 750, 2016.
- [2] R. Wang, M. S. H. Aung, S. Abdullah, R. Brian, A. T. Campbell, T. Choudhury, M. Hauser, J. Kane, M. Merrill, E. A. Scherer, V. W. S. Tseng, and D. Ben-Zeev, "Crosscheck: Toward passive sensing and detection of mental health changes in people with schizophrenia," in *Proceedings of the 2016 ACM International Joint Conference on Pervasive and Ubiquitous Computing*. ACM, 2016, p. 886–897.
- [3] D. C. Mohr, M. Zhang, and S. M. Schueller, "Personal sensing: understanding mental health using ubiquitous sensors and machine learning," *Annual review of clinical psychology*, vol. 13, pp. 23–47, 2017.
- [4] Z. Chen, M. Lin, F. Chen, N. D. Lane, G. Cardone, R. Wang, T. Li, Y. Chen, T. Choudhury, and A. T. Campbell, "Unobtrusive sleep monitoring using smartphones," in *7th International Conference on Pervasive Computing Technologies for Healthcare and Workshops*. IEEE, 2013, pp. 145–152.
- [5] A. Bulling, U. Blanke, and B. Schiele, "A tutorial on human activity recognition using body-worn inertial sensors," *ACM Computing Surveys (CSUR)*, vol. 46, no. 3, pp. 1–33, 2014.
- [6] K. Hänsel, R. Poguntke, H. Haddadi, A. Alomainy, and A. Schmidt, "What to put on the user: Sensing technologies for studies and

- physiology aware systems," in *Proceedings of the 2018 CHI Conference on Human Factors in Computing Systems*, 2018, pp. 1–14.
- [7] E. Reinertsen and G. D. Clifford, "A review of physiological and behavioral monitoring with digital sensors for neuropsychiatric illnesses," *Physiological measurement*, vol. 39, no. 5, p. 05TR01, 2018.
 - [8] E. L. Shepard, R. P. Wilson, L. G. Halsey, F. Quintana, A. G. Laich, A. C. Gleiss, N. Liebsch, A. E. Myers, and B. Norman, "Derivation of body motion via appropriate smoothing of acceleration data," *Aquatic Biology*, vol. 4, no. 3, pp. 235–241, 2008.
 - [9] K. Katevas, I. Leontiadis, M. Pielot, and J. Serrà, "Practical processing of mobile sensor data for continual deep learning predictions," in *Proceedings of the 1st International Workshop on Deep Learning for mobile systems and applications*, 2017, pp. 19–24.
 - [10] J. Wang, Y. Chen, S. Hao, X. Peng, and L. Hu, "Deep learning for sensor-based activity recognition: A survey," *Pattern Recognition Letters*, vol. 119, pp. 3–11, 2019.
 - [11] J. Yang, M. N. Nguyen, P. P. San, X. L. Li, and S. Krishnaswamy, "Deep convolutional neural networks on multichannel time series for human activity recognition," in *Twenty-Fourth International Joint Conference on Artificial Intelligence*, 2015.
 - [12] C. A. Ronao and S.-B. Cho, "Human activity recognition with smartphone sensors using deep learning neural networks," *Expert systems with applications*, vol. 59, pp. 235–244, 2016.
 - [13] A. Ignatov, "Real-time human activity recognition from accelerometer data using convolutional neural networks," *Applied Soft Computing*, vol. 62, pp. 915–922, 2018.
 - [14] F. Ordóñez and D. Roggen, "Deep convolutional and LSTM recurrent neural networks for multimodal wearable activity recognition," *Sensors*, vol. 16, no. 1, p. 115, 2016.
 - [15] Y. Zhao, R. Yang, G. Chevalier, X. Xu, and Z. Zhang, "Deep residual bidir-LSTM for human activity recognition using wearable sensors," *Mathematical Problems in Engineering*, vol. 2018, 2018.
 - [16] S. Yao, S. Hu, Y. Zhao, A. Zhang, and T. Abdelzaher, "Deepsense: A unified deep learning framework for time-series mobile sensing data processing," in *Proceedings of the 26th International Conference on World Wide Web*, 2017, pp. 351–360.
 - [17] J. V. Jeyakumar, L. Lai, N. Suda, and M. Srivastava, "Sensehar: a robust virtual activity sensor for smartphones and wearables," in *Proceedings of the 17th Conference on Embedded Networked Sensor Systems*, 2019, pp. 15–28.
 - [18] M. Malekzadeh, R. G. Clegg, A. Cavallaro, and H. Haddadi, "Privacy and utility preserving sensor-data transformations," *Pervasive and Mobile Computing*, 2020.
 - [19] D. Chu, N. D. Lane, T. T.-T. Lai, C. Pang, X. Meng, Q. Guo, F. Li, and F. Zhao, "Balancing energy, latency and accuracy for mobile sensor data classification," in *Proceedings of the 9th ACM Conference on Embedded Networked Sensor Systems*, 2011, pp. 54–67.
 - [20] Y. Liang, X. Zhou, Z. Yu, and B. Guo, "Energy-efficient motion related activity recognition on mobile devices for pervasive healthcare," *Mobile Networks and Applications*, vol. 19, no. 3, pp. 303–317, 2014.
 - [21] A. Raij, A. Ghosh, S. Kumar, and M. Srivastava, "Privacy risks emerging from the adoption of innocuous wearable sensors in the mobile environment," in *Proceedings of the SIGCHI Conference on Human Factors in Computing Systems*, 2011, pp. 11–20.
 - [22] M. Malekzadeh, R. G. Clegg, A. Cavallaro, and H. Haddadi, "Mobile sensor data anonymization," in *Proceedings of the International Conference on Internet of Things Design and Implementation (IoTDI)*. ACM, 2019, pp. 49–58.
 - [23] P. K. Choubey, S. Pateria, A. Saxena, V. P. C. SB, K. K. Jha, and S. B. PM, "Power efficient, bandwidth optimized and fault tolerant sensor management for iot in smart home," in *2015 IEEE International Advance Computing Conference (IACC)*. IEEE, 2015, pp. 366–370.
 - [24] A. Mathur, A. Isopoussu, N. Berthouze, N. D. Lane, and F. Kawsar, "Unsupervised domain adaptation for robust sensory systems," in *Adjunct Proceedings of the 2019 ACM International Joint Conference on Pervasive and Ubiquitous Computing and Proceedings of the 2019 ACM International Symposium on Wearable Computers*, 2019, pp. 505–509.
 - [25] L. Köping, K. Shirahama, and M. Grzegorzec, "A general framework for sensor-based human activity recognition," *Computers in biology and medicine*, vol. 95, pp. 248–260, 2018.
 - [26] P. Zappi, C. Lombriser, T. Stiefmeier, E. Farella, D. Roggen, L. Benini, and G. Tröster, "Activity recognition from on-body sensors: accuracy-power trade-off by dynamic sensor selection," in *European Conference on Wireless Sensor Networks*. Springer, 2008, pp. 17–33.
 - [27] D. Gordon, J. Czerny, T. Miyaki, and M. Beigl, "Energy-efficient activity recognition using prediction," in *2012 16th International Symposium on Wearable Computers*. IEEE, 2012, pp. 29–36.
 - [28] X. Zhu, Q. Li, and G. Chen, "Apt: Accurate outdoor pedestrian tracking with smartphones," in *2013 Proceedings IEEE INFOCOM*. IEEE, 2013, pp. 2508–2516.
 - [29] H. Ghasemzadeh, N. Amini, R. Saeedi, and M. Sarrafzadeh, "Power-aware computing in wearable sensor networks: An optimal feature selection," *IEEE Transactions on Mobile Computing*, vol. 14, no. 4, pp. 800–812, 2014.
 - [30] S. Saeedi and N. El-Sheimy, "Activity recognition using fusion of low-cost sensors on a smartphone for mobile navigation application," *Micromachines*, vol. 6, no. 8, pp. 1100–1134, 2015.
 - [31] X. Yang, Y. Chen, H. Yu, Y. Zhang, W. Lu, and R. Sun, "Instance-wise dynamic sensor selection for human activity recognition," in *Proceedings of the AAAI Conference on Artificial Intelligence*, vol. 34, no. 01, 2020, pp. 1104–1111.
 - [32] X. Qi, M. Keally, G. Zhou, Y. Li, and Z. Ren, "Adasense: Adapting sampling rates for activity recognition in body sensor networks," in *2013 IEEE 19th Real-Time and Embedded Technology and Applications Symposium (RTAS)*. IEEE, 2013, pp. 163–172.
 - [33] A. Khan, N. Hammerla, S. Mellor, and T. Plötz, "Optimising sampling rates for accelerometer-based human activity recognition," *Pattern Recognition Letters*, vol. 73, pp. 33–40, 2016.
 - [34] W. Cheng, S. Erfani, R. Zhang, and R. Kotagiri, "Learning datum-wise sampling frequency for energy-efficient human activity recognition," in *Thirty-Second AAAI Conference on Artificial Intelligence*, 2018.
 - [35] E. Walton, C. Casey, J. Mitsch, J. A. Vázquez-Diosdado, J. Yan, T. Dottorini, K. A. Ellis, A. Winterlich, and J. Kaler, "Evaluation of sampling frequency, window size and sensor position for classification of sheep behaviour," *Royal Society open science*, vol. 5, no. 2, p. 171442, 2018.
 - [36] J. Hounslow, L. Brewster, K. Lear, T. Guttridge, R. Daly, N. Whitney, and A. Gleiss, "Assessing the effects of sampling frequency on behavioural classification of accelerometer data," *Journal of experimental marine biology and ecology*, vol. 512, pp. 22–30, 2019.
 - [37] H.-H. Hsu, C.-T. Chu, Y. Zhou, and Z. Cheng, "Two-phase activity recognition with smartphone sensors," in *2015 18th International Conference on Network-Based Information Systems*. IEEE, 2015, pp. 611–615.
 - [38] J.-H. Choi and J.-S. Lee, "Embracenet: A robust deep learning architecture for multimodal classification," *Information Fusion*, vol. 51, pp. 259–270, 2019.
 - [39] S. Richoz, L. Wang, P. Birch, and D. Roggen, "Transportation mode recognition fusing wearable motion, sound and vision sensors," *IEEE Sensors Journal*, 2020.
 - [40] Z. Yan, V. Subbaraju, D. Chakraborty, A. Misra, and K. Aberer, "Energy-efficient continuous activity recognition on mobile phones: An activity-adaptive approach," in *2012 16th international symposium on wearable computers*. IEEE, 2012, pp. 17–24.
 - [41] G. W. Corder and D. I. Foreman, *Nonparametric statistics: A step-by-step approach*. John Wiley & Sons, 2014.
 - [42] I. Goodfellow, Y. Bengio, and A. Courville, *Deep learning*. MIT press, 2016.
 - [43] J. Long, E. Shelhamer, and T. Darrell, "Fully convolutional networks for semantic segmentation," in *Proceedings of the IEEE conference on computer vision and pattern recognition*, 2015, pp. 3431–3440.
 - [44] Y. Bengio, A. Courville, and P. Vincent, "Representation learning: A review and new perspectives," *IEEE transactions on pattern analysis and machine intelligence*, vol. 35, no. 8, pp. 1798–1828, 2013.
 - [45] J. Ae Lee and J. Gill, "Missing value imputation for physical activity data measured by accelerometer," *Statistical methods in medical research*, vol. 27, no. 2, pp. 490–506, 2018.
 - [46] E. Quiring, D. Klein, D. Arp, M. Johns, and K. Rieck, "Adversarial preprocessing: Understanding and preventing image-scaling attacks in machine learning," in *29th USENIX Security Symposium (USENIX Security 20)*. USENIX Association, 2020, pp. 1363–1380.
 - [47] M. Lin, Q. Chen, and S. Yan, "Network in network," in *Proceedings of the 2nd International Conference on Learning Representations, ICLR*, 2014.
 - [48] K. He, X. Zhang, S. Ren, and J. Sun, "Spatial pyramid pooling in deep convolutional networks for visual recognition," *IEEE transactions on pattern analysis and machine intelligence*, vol. 37, no. 9, pp. 1904–1916, 2015.
 - [49] M. G. Abdu-Aguye and W. Gomaa, "Versatl: versatile transfer learning for imu-based activity recognition using convolutional

- neural networks," in *The 16th International Conference on Informatics in Control, Automation and Robotics (ICINCO)*, 2019.
- [50] H. Zhao, J. Shi, X. Qi, X. Wang, and J. Jia, "Pyramid scene parsing network," in *Proceedings of the IEEE conference on computer vision and pattern recognition*, 2017, pp. 2881–2890.
 - [51] S. Hochreiter and J. Schmidhuber, "Long short-term memory," *Neural computation*, vol. 9, no. 8, pp. 1735–1780, 1997.
 - [52] F. Karim, S. Majumdar, H. Darabi, and S. Chen, "LSTM fully convolutional networks for time series classification," *IEEE access*, vol. 6, pp. 1662–1669, 2017.
 - [53] K. Bonawitz, H. Eichner, W. Grieskamp, D. Huba, A. Ingerman, V. Ivanov, C. Kiddon, J. Konecny, S. Mazzocchi, H. B. McMahan, T. Van Overveldt, D. Petrou, D. Ramage, and J. Roselander, "Towards federated learning at scale: System design," in *Proceedings of the 2nd SysML Conference, Palo Alto, CA, USA*, 2019.
 - [54] C. Finn, P. Abbeel, and S. Levine, "Model-agnostic meta-learning for fast adaptation of deep networks," in *Proceedings of the 34th International Conference on Machine Learning-Volume 70*. JMLR. org, 2017, pp. 1126–1135.
 - [55] A. Nichol, J. Achiam, and J. Schulman, "On first-order meta-learning algorithms," *arXiv preprint [arXiv:1803.02999](https://arxiv.org/abs/1803.02999)*, 2018.
 - [56] R. M. French, "Catastrophic forgetting in connectionist networks," *Trends in cognitive sciences*, vol. 3, no. 4, pp. 128–135, 1999.
 - [57] N. Qian, "On the momentum term in gradient descent learning algorithms," *Neural networks*, vol. 12, no. 1, pp. 145–151, 1999.
 - [58] D. P. Kingma and J. Ba, "Adam: A method for stochastic optimization," in *Proceedings of the 3rd International Conference on Learning Representations (ICLR)*, 2014.
 - [59] D. Anguita, A. Ghio, L. Oneto, X. Parra, and J. L. Reyes-Ortiz, "A public domain dataset for human activity recognition using smartphones." in *Proceedings of the 21st European Symposium on Artificial Neural Networks, Computational Intelligence and Machine Learning, ESANN*, April 2013, pp. 437–442.
 - [60] G. Vavoulas, C. Chatzaki, T. Malliotakis, M. Pediaditis, and M. Tsiknakis, "The mobiaact dataset: Recognition of activities of daily living using smartphones." in *ICT4AgeingWell*, 2016, pp. 143–151.
 - [61] M. Malekzadeh, R. G. Clegg, A. Cavallaro, and H. Haddadi, "Protecting sensory data against sensitive inferences," in *Proceedings of the 1st Workshop on Privacy by Design in Distributed Systems*, ser. W-P2DS'18. ACM, 2018, pp. 2:1–2:6.
 - [62] M. Shoaib, S. Bosch, O. D. Incel, H. Scholten, and P. J. Havinga, "Complex human activity recognition using smartphone and wrist-worn motion sensors," *Sensors*, vol. 16, no. 4, p. 426, 2016.
 - [63] M. Abadi, P. Barham, J. Chen, Z. Chen, A. Davis, J. Dean, M. Devin, S. Ghemawat, G. Irving, M. Isard *et al.*, "Tensorflow: A system for large-scale machine learning," in *12th USENIX Symposium on Operating Systems Design and Implementation (OSDI 16)*, 2016, pp. 265–283.
 - [64] N. Srivastava, G. Hinton, A. Krizhevsky, I. Sutskever, and R. Salakhutdinov, "Dropout: a simple way to prevent neural networks from overfitting," *The journal of machine learning research*, vol. 15, no. 1, pp. 1929–1958, 2014.
 - [65] T. Tieleman and G. Hinton, "Lecture 6.5-rmsprop: Divide the gradient by a running average of its recent magnitude," *COURSERA: Neural networks for machine learning*, vol. 4, no. 2, pp. 26–31, 2012.